Applied Surface Science 255 (2009) 4056–4060

Contents lists available at ScienceDirect

Applied Surface Science

journal homepage: www.elsevier.com/locate/apsusc

Effect of contact angle hysteresis on water droplet evaporation from super-hydrophobic surfaces

S.A. Kulinich *, M. Farzaneh

CIGELE/INGIVRE, Department of Applied Sciences, Université du Québec à Chicoutimi, 555 University Blvd., Saguenay, PQ, Canada G7H 2B1

ARTICLE INFO

Article history:
Received 30 June 2008
Received in revised form 1 October 2008
Accepted 26 October 2008
Available online 7 November 2008

Keywords:
Super-hydrophobicity
Wetting hysteresis
Evaporation
Surface roughness

ABSTRACT

Small water drops demonstrate different evaporation modes on super-hydrophobic polymer surfaces with different hysteresis of contact angle. While on the high-hysteresis surface evaporation follows the constant-contact-diameter mode, the constant-contact-angle mode dominates on the low-hysteresis surface. These modes were previously reported for smooth hydrophilic and hydrophobic surfaces, respectively. The experimental data are compared to the previous models describing spherical cap drops that evaporate in different modes, and good fitting is obtained.

1. Introduction

There has been significant interest in recent years in development of super water-repellent surfaces, which exhibit water contact angles (CAs) larger than 150° [1–10]. Such surfaces show potential in a variety of applications from anti-sticking, anti-contamination and self-cleaning to anti-corrosive, frost- and snow-repellent, low-friction coatings, among others [6–14]. In parallel, studies on the dynamic behavior of such surfaces have been attracting more and more interest [10,11,13–17]. This can partly be explained by the recent belief that the static hydrophobicity alone is not sufficient to fully characterize the wetting properties of surfaces [10,16–18].

Free evaporation of small water droplets from various surfaces is an apparently simple problem related to the dynamic behavior of such systems, with relevance to both academic and practical interests. However, more complete knowledge of how evaporation influences the CA and water drop shape is still necessary for better understanding numerous dynamic wetting/dewetting processes on surfaces. That knowledge is also very important in the wetting and surface characterization processes as CA, being an important parameter characterizing surface properties, appears to change when inevitable evaporation of water in air occurs.

While extensive studies have been carried out on the evaporation of water droplets from solids [19–26], relatively little research has been done on hydrophobic surfaces [20,23,24,26], and even less so on super-hydrophobic surfaces [26–28]. McHale and co-workers studied evaporation on a super-hydrophobic surface formed by regularly patterned polymer and having high CA hysteresis (CAH) [26]. It was shown that water droplets initially evaporated in a pinned contact line (i.e. so-called constant-contact-diameter, CD) mode, before the contact line receded in a stepwise fashion, jumping from pillar to pillar of the patterned surfaces [26]. An abrupt collapse of some droplets into the pillar structure was observed in some cases during evaporation, while other droplets appeared to collapse into the structure only at very late stages of evaporation, which could not be detected by the optics used [26]. Zhang et al. [27] followed sessile water droplets evaporating on super-hydrophobic lotus leaf and biomimetic polymer surfaces. Both hierarchically structured samples demonstrated the constant-CD mode of evaporation, while CAH values were not evaluated. Most recently, Reyssat et al. followed drop evaporation on Si wafers decorated with regular cylindrical micropillars and passivated with a fluoropolymer, where CAH values were ~20–25° [28]. They observed mainly constant CA during the first stage of evaporation, while at later stages drops could collapse into the structure (with shorter pillars) or remain suspended to the very end (on taller pillars) [28]. Evaporation from disordered (i.e. opposed to regularly patterned) super-hydrophobic surfaces with very low values of CAH has not been reported thus far.

* Corresponding author.
E-mail address: skulinic@uqac.ca (S.A. Kulinich).

0169-4332/$ – see front matter.
doi:10.1016/j.apsusc.2008.10.109

Two conditions for a small water drop determining the behavior of its CA and CD during evaporation from a smooth surface were previously reported in the literature [19–22,24]. More specifically, on wetting solids with CA $<90^\circ$, evaporation rate was observed to be linear with time, with CA decreasing and CD remaining constant (the constant-CD mode) [19–23]. On non-wetting solids, the rate of evaporation was found to be non-linear, since CA remains constant, while CD decreases (the constant-CA mode) [20,24]. It was suggested that CAH is a factor influencing drop evaporation, in particular on rough surfaces [20,23,25,29], but no systematic work has been conducted thus far to elucidate its effect.

In this study, two surfaces with similar values of CA ($\geq 150^\circ$) and surface chemistry (passivated with a fluoropolymer) but contrasting wetting hysteresis were prepared. It is experimentally shown that a high value of CA itself does not determine the evaporation behavior of sessile water droplets on such samples. And it is rather the wetting hysteresis (or the receding CA) that governs the evaporation mode. Depending on pinning ability, the super-hydrophobic surfaces (with similar chemistry) followed the evaporation modes previously reported for smooth hydrophobic or hydrophilic surfaces.

2. Experimental details

Prior to coating, aluminium plates (AA6061, 1 in. × 1 in.) were polished with emery paper and cleaned in organic solvents. ZrO_2 nanopowder (3.0 g) with an average size of 20–30 nm from Aldrich was mixed with 40 ml of deionized water. The suspension was sonicated for 30 min, after which 2.4 ml of a perfluoroalkyl methacrylic copolymer (Zonyl 8740, DuPont) product were added. The final suspension was stirred for another 3 h before coating on the substrates. Super-hydrophobic sample 1 was prepared by spraying the suspension over the substrate surface uniformly and letting it dry at ~50 °C. Super-hydrophobic sample 2 was prepared by spin-coating of the same suspension on the substrate. Upon coating, the samples were heat-treated at 120 °C in air for 3 h to remove residual solvents.

Contact angles were measured by the sessile-drop method on a Krüss DSA10 contact-angle goniometer; the values reported herein were the average of at least five measurements on various parts of each sample. They were recorded at 23 ± 0.5 °C with distilled water; all droplets were 4 μL in volume. The same instrument was used to observe water droplet evolution over time as a result of evaporation. Long-term behavior of water drops on the surfaces was evaluated by measuring the evolution of their contact angle and contact diameter on each surface for periods of time up to ~43 min (until the droplets could be detected by the optics). Several droplets were observed during their evaporation on each sample, showing good statistical consistency. The evaporation curves presented here were chosen as typical for each sample.

Advancing contact angles were measured after sequential deposition with a small syringe and needle. A small drop was deposited on the surface, and then additional water was added to advance the contact line. The needle was inserted into the drop during injection to prevent drops from move on the super water-repellent surface 2. For receding contact angles, water was withdrawn until the contact line retracted. Measurements were made on both sides of more than five droplets and than averaged. Scanning electron microscopy (SEM) of the sample surfaces was carried out with a JSM-6330-F microscope (JEOL) after coating them with a thin conducting layer of Pt. Topography of the sample surfaces was analyzed with a WYKO NT1100 optical profilometer (Veeco). X-ray photoelectron spectroscopy (XPS) was performed with a Quantum-2000 instrument from ULVAC-PHI.

3. Results and discussion

Several sources of wetting hysteresis are normally recognized in the literature. Amongst such, the major ones are considered to be either chemical (e.g. inhomogeneity of chemical composition of the solid surface) or physical (of which roughness is probably the most known) [8,21,28,30-32]. Therefore, to prepare super-hydrophobic surfaces with different CAH, roughness of the samples was varied by depositing fluoropolymer coatings, into which ZnO_2 nanoparticles were incorporated, through either spray-coating (sample 1) or spin-coating (sample 2). This led to different surface roughness and CAH characteristics of the samples (see Figs. 1 and 2). Both samples exhibit super-hydrophobic properties with very close values of CA in the range of ~152–153°. At the same time, as seen in Figs. 1b and 2b (insets), the CAH values of the samples are very different, being >70° and ~5° for samples 1 and 2, respectively. Thus, of the two samples prepared, one demonstrates a "sticky" state (1) and the other "slippy" state (2) for water droplets on their surfaces [4,8,9,30,31]. As seen from the SEM images in Fig. 1a, asperities are less separated and have larger surface area in sample 1, with their tops being relatively flat and shallow. Therefore, water drops are expected to have larger water–solid contact area on this surface, leading to the high CAH observed in Fig. 1b (inset) and "sticky" state [4,30,31]. Meanwhile, sharper and better separated asperities are observed in the SEM surface images of sample 2 (Fig. 2a), which is normally associated with lower CAH and "slippy" state of hydrophobic surfaces [4,30,31]. Comparison of surface profiles of the samples (Figs. 1b and 2b) also confirms that the asperities in sample 2 are better separated and taller, giving rise to larger surface roughness. The root mean square roughness value of sample 2 was evaluated by optical profilometry to be ~419 nm, which is larger than that of sample 1 (~257 nm). Since these values are only different by a factor of ~2, the big

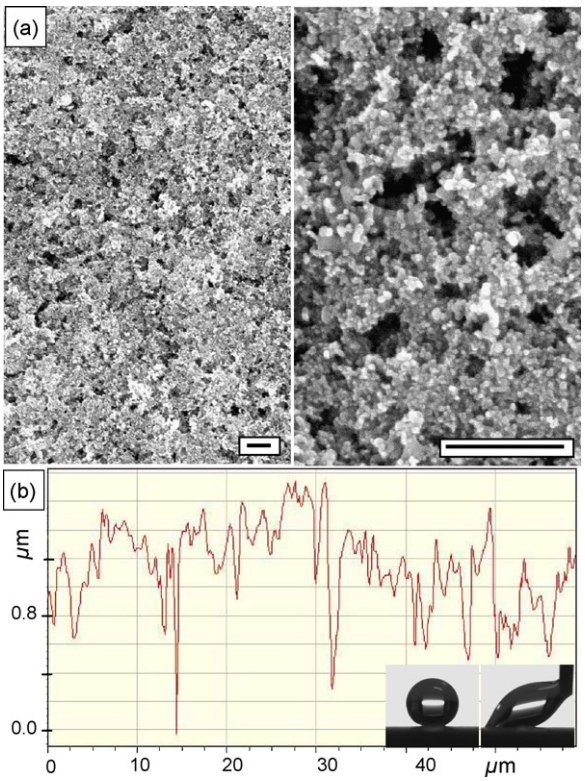

Fig. 1. Surface images at different magnification (a) and surface profile (b) of sample 1. Sessile and moving (with a needle) water droplets (4 μL) are shown as insets. CA value is 152.1° ± 3.5°, CAH value is >70°. Scale bars indicate 500 nm.

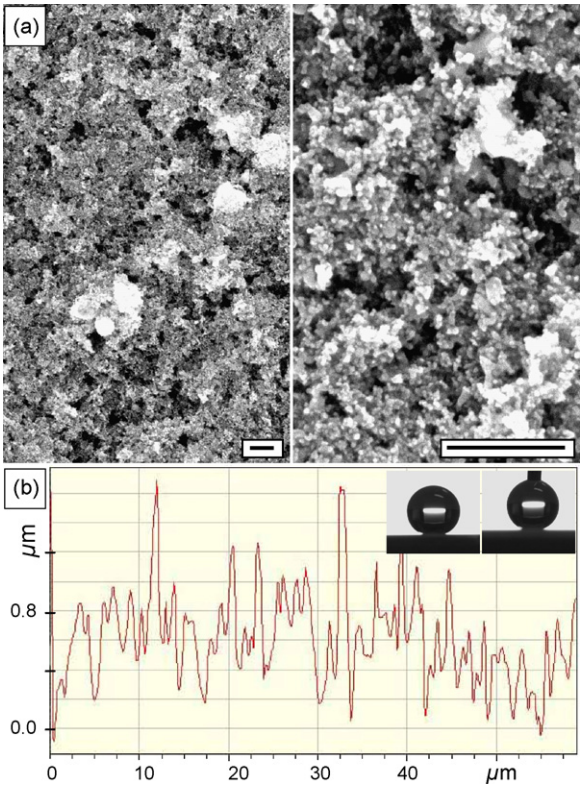

Fig. 2. Surface images at different magnification (a) and surface profile (b) of sample 2. Sessile and moving (with a needle) water droplets (4 μL) are shown as insets. CA value is 153.3° ± 1.5°, CAH value is 4.9° ± 1.7°. Scale bars indicate 500 nm.

difference in the CAH values observed is believed to be resulted from the different wetting regimes realized on the samples. While sample 2 demonstrates all features of the Cassie–Baxter wetting [7–10,12,32,33] (with water droplet sitting on tops of solid asperities), the wetting regime on sample 1 is believed to be a mixed (i.e. Wenzel [7,8,10,12,32,34] and Cassie–Baxter) one. This implies coexistence of both air entrapment and large water–solid contact area on the rough surface and leads to both the high CA and strong pinning observed.

Since both samples exhibit CA >150°, it is safe to conclude that oxide nanoparticles only help form surface roughness, while it is the fluoropolymer that is in the topmost layer all over the surface. That is, both samples have similar surface chemistry, and it is their surface roughness that is responsible for the difference in dynamic hydrophobicity observed. This is supported by XPS analysis (results not shown here). Only F, Zr, C, O and Al peaks are seen in both XPS survey spectra. The atomic ratio of the elements present in the coatings, F:Zr:C:O, was equal to 1.2:0.91:10.09:4.83 and 1.24:1.01:11.93:5.35 for samples 1 and 2, respectively.

Fig. 3 compares changes in CA (a) and CD (b) for two droplets as they evaporate on samples 1 and 2. Fig. 4 shows schematically profile sequences for the same droplets on surfaces 1 (a) and 2 (b), corresponding to evaporation times of 1, 20, 27, 34 and 37 min. As seen in Fig. 3a, the initial values of CA were both slightly greater than 150°, and the corresponding values of CD in Fig. 3b were also very close, being about 0.92 and 0.86 mm for samples 1 and 2, respectively. Thus, the initial geometric parameters of the droplets, related to the static hydrophobicity of the surfaces, were comparable.

The CA of the droplet on surface 1 is seen to steadily decrease over time in Fig. 3a, while its CD remains approximately constant up to ~2260 s (when CD is observed to be ~0.77 mm). After this, a

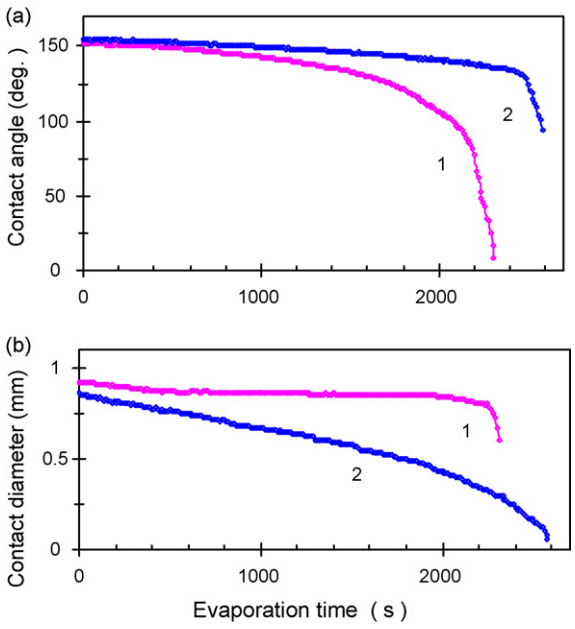

Fig. 3. Evolution of contact angle (a) and contact diameter (b) of water droplets (4 μL) evaporating on surfaces 1 and 2.

fast decrease in CD is observed till ~2310 s, when the last measurement on sample 1 was possible, resulting in a CD value of about 0.6 mm, as shown in Fig. 3b. In contrast, the droplet on surface 2 exhibits a smooth decrease in its CD, and the last measurement at ~2580 s gives a value as small as 0.06 mm, which is about one order of magnitude lower than that observed on sample 1 (see Fig. 3b). In agreement with the typical constant-CA mode observed on hydrophobic surfaces by others [20,24], a quasi-static CA–time dependence is observed up to ~2450 s for sample 2, as seen in Fig. 3a, after which a steep slope is observed with the last measurement at ~2580 s showing CA ~90° (Fig. 4b, inset). The evaporation on sample 1 ends after ~2310 s, when the last CA observed is lower than 10° (Fig. 4a, inset). Note that time dependencies similar to those in Fig. 3a and b have been observed for all droplets studied.

All the above peculiarities of the dynamic behavior of water drops on the high-CAH surface 1 appear to be related to its high "sticky" ability, which is associated with its very low value of receding CA (see inset in Fig. 1b). As the contact line is not mobile and tends to be pinned on this surface, when evaporation proceeds, it must be accompanied by a reduction in CA, which is well seen in Fig. 4a. This contrasts sharply the behavior of droplets on the low-CAH surface 2, where the contact line is very mobile (CAH ~5°) so that it moves quickly as evaporation proceeds and droplet volume

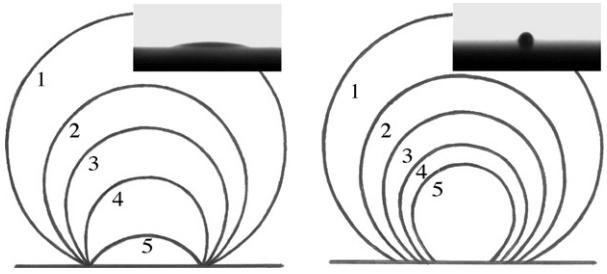

Fig. 4. Schematic shape evolution of water droplets during evaporation from surfaces 1 (a) and 2 (b). Droplet profiles are shown for 1 (1), 20 (2), 27 (3), 34 (4) and 37 min (5). Insets are photographs of droplets just a few seconds before disappearance.

goes down (Fig. 4b). This contact line motion without pinning on surface heterogeneities is believed to sustain the observed quasi-static CA evaporation as the dominating mode on sample 2. It is clearly seen in Figs. 4a and b (insets) that even just a few seconds before vanishing, a droplet on sample 1 is much pinned and exhibits very low CA, whereas one on sample 2 has a much smaller contact area and higher CA. It is thus seen that a high value of CA $\geq$150° itself does not determine the evaporation behavior of water drops on the surface. Whether the drop follows the constant-CD or constant-CA mode, depends on the surface ability to pin the drop (i.e. receding CA). Interestingly, the constant-CD mode was observed on a super-hydrophobic surface with a low receding CA; this mode was previously ascribed to smooth hydrophilic surfaces [19–23].

Furthermore, the difference in the contact line motion (pinned or mobile behavior) appears to be responsible for the different life-times of the droplets observed in Fig. 3. As the CA of the pinned droplet (Fig. 3a, curve 1) approaches 90°, and eventually drops below this value, evaporation through the entire water–air interface must become possible as a shape of a droplet with CA <90° cannot hinder any air circulation near the contact line any longer [24]. As the evaporation depends on vapor diffusion into surrounding atmosphere, it was reported to be limited near the contact line of droplets with CA >90°, since air circulation is geometrically limited there [24]. Therefore, as the shape of drop 1 gradually turns into that with CA <90°, the droplet mass loss is expected to increase if compared to that of drop 2, which essentially keeps its CA >90° all the time (see Fig. 3a, curve 2). This inevitably leads to the shorter life-time of drop 1. The profiles in Fig. 4 are well consistent with the above explanation. Indeed, while profiles 4, representing shape of the drops after 34 min, appear to be comparable in terms of droplet volume, a big mass loss is observed between 34 and 37 min (profiles 4 and 5) in Fig. 4a, when the droplet on the high-CAH surface has reached CA values <90°. At the same time, the volume change between profiles 4 and 5 in Fig. 4b is obviously smaller, thus confirming a slower evaporation rate from the lower part of the droplet which holds its CA >90°. It is also reasonable to assume that the free energy of drop 1, which is more distorted from its equilibrium shape, is higher than that of drop 2. This could also contribute to its faster evaporation.

Since no ellipsoidal cap analysis has been previously provided for drops evaporating in the constant-CA mode, in Fig. 5 we only analyze how the experimental data in Fig. 3 fit two previously developed models describing the evaporation of spherical cap droplets. A clear linearity of the experimental r^2 (square of contact radius) values over time for the data set of sample 2 is well recognized, implying that the diffusion model of McHale et al. [24,35] (more specifically, the extension for the non-wetting case with a quasi-static CA as the dominant stage) works well for the evaporation observed on the low-CAH super-hydrophobic sample 2. According to the model, the r^2 of a spherical cap drop on a non-wetting surface, provided that CA changes slowly, can be described by the following equation:

$$r^2 = C - \frac{4D\Delta c t \sin^2\theta}{\rho(1-\cos\theta)(2+\cos\theta)} \quad (1)$$

where C is a constant of integration, D is the diffusion coefficient of the vapor, ρ is the density of water, $\theta = \theta(t)$ is the CA, $\Delta c = (c_s - c_\infty)$ is the difference between the vapor concentration at the drop surface and the ambient value far removed from the surface, and t is time.

The evaporation of spherical cap droplets with constant CD and CA >90° was proposed to be analyzed by plotting the function $H_{PB}(\theta)$ against time [26]. This function is defined by the following equation.

$$H_{PB}(\theta) \equiv \frac{-e_0}{1+u} + e_1 \ln(1+u) + e_2 u + e_3 u^2 = \frac{-2D\Delta c t}{\rho r^2} + H_{PB}(\theta_0) \quad (2)$$

where $u(t) = \cos\theta(t)$, e_0, e_1, e_2 and e_3 are constants (given in [26] and valid for $90° < \theta < 180°$), and $H_{PB}(\theta_0)$ is a constant of integration representing the function value at $t = 0$ [26]. As seen in Fig. 5, the data set for sample 1 can be fitted well to a straight line, indicating the linear time dependence of the experimental $H_{PB}(\theta)$ values. Some deviation from linearity is seen at times before ~600 s (when CD of droplet 1 slightly changes, as seen in Fig. 3b) and after ~2200 s (when CA drops below 90° and the model is not valid any longer). It is thus seen that both Eqs. (1) and (2) are valid for the evaporation observed in this study on low-CAH and high-CAH surfaces, respectively. On the other hand, theoretical approaches based on ellipsoidal cap droplets are expected to give better fits, since the drops had some eccentricity (e ~0.35).

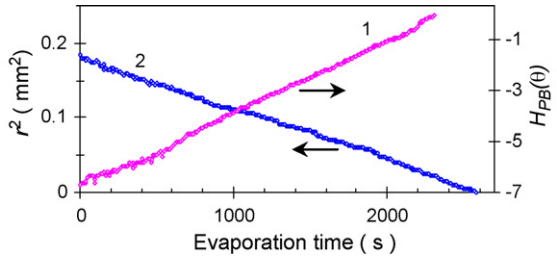

Fig. 5. Tests of Eq. (1) (curve 2) and (2) (curve 1) for the data presented in Fig. 3.

4. Conclusions

The evaporation of small water droplets on super-hydrophobic surfaces (CA > 150°) with similar surface chemistry has been shown to follow different modes, depending on pinning ability of surfaces. More specifically, the surface with a low CAH was observed to follow the evaporation model normally ascribed to hydrophobic surfaces (quasi-static CA while constantly decreasing CD for most of the evaporation time). Meanwhile, the surface with a high CAH was found to behave in accordance with the evaporation model normally associated with hydrophilic surfaces (constantly decreasing CA and quasi-static CD). Water droplets were observed to evaporate faster on the surface with high CAH. This is attributed to the fact that high values of CA >90° are sustained on the low-hysteresis surface for much longer periods of time, and the evaporation rate of such droplets is likely to be suppressed in the area close to the contact line. Local saturation vapor is generated near the contact line which hinders evaporation. In contrast, drops on the high-hysteresis surface reached values CA <90° faster, from which point in time evaporation takes place from the entire water–air interface. The experimental data obtained compare well with the previous theoretical analysis of spherical cap drops evaporating in different modes.

Acknowledgments

This work was supported by Hydro-Québec, Hydro One, Alcan Cable, K-Line Insulators, Électricité de France, CQRDA and FUQAC. The authors also thank Dr. K. Nose (Univ. Tokyo) for his help with SEM and XPS analyses.

References

[1] A. Qu, X.F. Wen, P.H. Pi, J. Cheng, Z. Yang, Appl. Surf. Sci. 253 (2007) 9430–9434.
[2] T.Y. Han, J.F. Shr, C.F. Wu, C.T. Hsieh, Thin Solid Films 515 (2007) 4666–4669.

[3] L. Gao, T.J. McCarthy, J. Am. Chem. Soc. 128 (2006) 9052–9053.
[4] Z.-G. Guo, W.-M. Liu, Appl. Phys. Lett. 90 (2007) 223111.
[5] A. Cao, L.L. Cao, D. Gao, Appl. Phys. Lett. 91 (2007) 034102.
[6] G.R.J. Artus, S. Jung, J. Zimmermann, H.-P. Gautschi, K. Marquardt, S. Seeger, Adv. Mater. 18 (2006) 2758–2762.
[7] A. Nakajima, K. Hashimoto, T. Watanabe, Monatsh. Chem. 132 (2001) 31–41.
[8] D. Quéré, Rep. Prog. Phys. 68 (2005) 2495–2532.
[9] X.M. Li, D. Reinhoudt, M. Crego-Calama, Chem. Soc. Rev. 36 (2007) 1350–1368.
[10] S.A. Kulinich, M. Farzaneh, Surf. Sci. 573 (2004) 379–390.
[11] H. Wang, L.M. Tang, X.M. Wu, W.T. Dai, Y.P. Qiu, Appl. Surf. Sci. 253 (2007) 8818–8824.
[12] S.A. Kulinich, M. Farzaneh, Vacuum 79 (2005) 255–264.
[13] Y.Y. Wu, N. Saito, F.A. Nae, Y. Inoue, O. Takai, Surf. Sci. 600 (2006) 3710–3714.
[14] S.A. Kulinich, M. Farzaneh, Appl. Surf. Sci. 230 (2004) 232–240.
[15] Z. Wang, C. Lopez, A. Hirsa, N. Koratkar, Appl. Phys. Lett. 91 (2007) 023105.
[16] M. Sakai, J.-H. Song, N. Yoshida, S. Suzuki, Y. Kameshima, A. Nakajima, Surf. Sci. 600 (2006) L204–L208.
[17] D. Öner, T.J. McCarthy, Langmuir 16 (2000) 7777–7782.
[18] W. Chen, A.Y. Fadeev, M.C. Hsieh, D. Öner, J. Youngblood, T.J. McCarthy, Langmuir 15 (1999) 3395–3399.
[19] K.S. Birdi, D.T. Vu, A. Winter, J. Phys. Chem. 93 (1989) 3702–3703.
[20] K.S. Birdi, D.T. Vu, J. Adhes. Sci. Technol. 7 (1993) 485–493.
[21] M.E.R. Shanahan, C. Bourgès, Int. J. Adhes. Adhes. 14 (1994) 201–205.
[22] S.M. Rowan, M.I. Newton, G. McHale, J. Phys. Chem. 99 (1995) 13268–13271.
[23] C. Bourgès-Monnier, M.E.R. Shanahan, Langmuir 11 (1995) 2820–2829.
[24] G. McHale, S.M. Rowan, M.I. Newton, M.K. Banerjee, J. Phys. Chem. B 102 (1998) 1964–1967.
[25] H.-Z. Yu, D.M. Soolaman, A.W. Rowe, J.T. Banks, ChemPhysChem 5 (2004) 1035–1038.
[26] G. McHale, S. Aqil, N.J. Shirtcliffe, M.I. Newton, H.Y. Erbil, Langmuir 21 (2005) 11053–11060.
[27] X.Y. Zhang, S.X. Tan, N. Zhao, X.L. Guo, X.L. Zhang, Y.J. Zhang, J. Xu, ChemPhysChem 7 (2006) 2067–2070.
[28] M. Reyssat, J.M. Yeomans, D. Quéré, Europhys. Lett. 81 (2008) 26006.
[29] H.Y. Erbil, G. McHale, S.M. Rowan, M.I. Newton, Langmuir 15 (1999) 7378–7385.
[30] C.W. Extrand, Langmuir 18 (2002) 7991–7999.
[31] G. McHale, N.J. Shirtcliffe, M.I. Newton, Langmuir 20 (2004) 10146–10149.
[32] H. Kusumaatmaja, J.M. Yeomans, Langmuir 23 (2007) 6019–6032.
[33] A.B.D. Cassie, S. Baxter, Trans. Faraday Soc. 40 (1944) 546–551.
[34] R.N. Wenzel, Ind. Eng. Chem. 28 (1936) 988–994.
[35] H.Y. Erbil, G. McHale, M.I. Newton, Langmuir 18 (2002) 2636–2641.